Advanced hyperthermia treatment: optimizing microwave energy focus for breast cancer therapy

Burak ACAR
burakacar2006@hotmail.com

TUBA YILMAZ ABDOLSAHEB
yilmaztub@gmail.com

Ali YAPAR
yapara@itu.edu.tr

Advanced hyperthermia treatment: optimizing microwave energy focus for breast cancer therapy

Burak ACAR[1*] , **Tuba YILMAZ**[2] , **Ali YAPAR**[3]

Department of Electronics and Communication Engineering, Istanbul Technical University, İstanbul, Turkiye

Abstract: This paper presents a fast antenna phase optimization scheme to enable microwave power focusing for breast cancer hyperthermia. The power focusing is achieved through the maximization of the deposited electric field on the target malignant tumor tissue. To do so, a malignant breast tumor, the surrounding breast medium, and the skin of the breast are modeled as a cylindrical structure composed of eccentric cylinders, and electric field distribution is computed analytically in terms of cylindrical harmonics. This approach minimized the computational cost and simplified the breast medium model. To ensure applicability across various breast types, the dielectric properties (DPs) of the main cylinder, symbolizing healthy breast tissue, are averaged from pixel DPs of digital breast phantoms. The hyperthermia problem is posed as maximizing the total electric field at the central point of the tumor which is simply represented as a vector sum of complex quantities in terms of antenna phases. That is, one antenna phase is selected as a reference and the remaining ones are adjusted accordingly. The approach is validated using a circular applicator with eight TMz polarized line sources surrounding realistic digital breast phantoms. Testing involved eight scenarios using two distinct breast media. In the optimal scenario, the peak temperature is achieved 1.3 mm away from the focus point.

Key words: Electromagnetics, microwave hyperthermia, antenna phase optimization, inverse problems, breast cancer treatment

1. Introduction

Microwave hyperthermia (MH) is utilized either as a sole or complementary method in noninvasive breast cancer treatment [1, 2]. As a sole treatment technique, it aims to selectively elevate the temperature of the malignant tumor tissue above 42 °C to enable cell necrosis on the tumor while maintaining the normal temperature at the surrounding healthy tissue [3, 4]. As a complementary method to chemotherapy, the application of MH aims to minimize the hypoxic regions on the malignant tumor by heating the tumor tissue a few degrees, thus increasing the effectiveness of the chemotherapy drugs [5].

For effective heating, the microwave power and thus the electric field must be concentrated on the target. Numerous studies have analyzed microwave power focusing for breast cancer hyperthermia using varied optimization algorithms and applicator configurations. Presented applicators are either equipped with arrays or individual antennas. Excitation optimization is carried out for subarrays or each antenna, depending on the hyperthermia applicator configuration. In [6], a breast cancer hyperthermia applicator equipped with linear antenna arrays is presented. The phases of the arrays were handled as two separate subarrays in which one array phase is selected as a reference, two array phases are selected as variables, and the remaining phase is

---

*Correspondence: burakacar2006@hotmail.com

represented as the sum of two variable array phases. Rather than using a traditional optimization function, a relationship between focus location and the antenna phases was established through simulations using a fading breast model. In [7], a two-step neural network optimization approach is presented for linear and circular applicators. The network is trained for excitation phases and next it is trained for the excitation amplitudes. This approach effectively optimizes excitation values for microwave energy focusing in the breast medium. Despite proposing a time- and cost-effective method to generate a large amount of data, the training time of the neural network increases with the number of antennas. Another study proposed optimizing both the excitations of antennas and the location of the applicator for breast cancer hyperthermia [8]. The proposed approach reduced the number of antennas while obtaining better metrics via the rotation of a linear system. The optimization is performed by using particle swarm optimization (PSO) algorithm. In another study [9], a two-step optimization scheme was proposed to focus microwave power in the breast medium through the optimization of antenna excitations. Firstly, phases of four square-arranged antenna arrays around the breast tissue were optimized using the trust-region algorithm. Secondly, subarray antenna amplitudes were optimized to raise the tumor's center temperature to $42\,^\circ$C. In [10], a system of linear antenna arrays with 6 elements stacked both in azimuth and elevation plane for breast cancer hyperthermia is presented. Having antenna arrays with elements located on the elevation plane enabled 3D focusing. Antenna element excitations were optimized using a PSO algorithm. Electric fields were calculated using Finite Element Modeling (FEM) software.

In other studies [11, 12], a breast cancer hyperthermia system with integrated thermoacoustic tomography for microwave power monitoring is presented. The proposed microwave hyperthermia system applicator consisted of a bowl-shaped breast encasing patch antennas to form a phased array. The antenna excitations were optimized by maximizing the ratio of power intensity on the tumor to the intensity on the healthy tissue through differential evolution. In [13], a concave microwave breast cancer hyperthermia applicator with integrated leaky-wave antennas is proposed to aid chemotherapy treatment. This work experimentally analyzed the temperature change of a realistic breast phantom at different depths by changing the magnitude of antenna excitation groups.

Other reported analysis in the literature includes a comparison of ultrawideband and narrowband focusing [14]. The effectiveness of 3D focusing is investigated in [15]. Real and imaginary parts of antenna excitations are considered as real parameters and optimized separately to maximize the field magnitude at the desired point in [16]. In [17], antenna phases in subarray groups surrounding a cylindrical breast medium were optimized to enable focusing. Yet in another study [18], a hyperthermia applicator with antenna arrays arranged in hexagonal fashion around the breast medium. Antenna excitation optimization was performed by maximizing the power transmission efficiency.

In another previous study [19], 2D FOCO (Optimal Constraint Power Focusing) approach is used in multifrequency for focusing with different breast models. Elkayal et al. [20] and Curto et al. [21] oriented their analysis towards temperature concentration rather than focusing on SAR with basic phantoms. In light of [4], Dooley et al. [22] extended Fenn's study and documented a clinical study involving the application of local anesthesia to the breast, followed by the insertion of a sensor catheter into a small incision. This sensor is responsible for monitoring both the electric field and temperature within the area. A beamforming technique was introduced for the purpose of noninvasive Microwave Hyperthermia in the context of pediatric brain cancer treatment in [23]. In [24], microwave hyperthermia technique is used for enhance the process of healing the muscle tissues postinjuries.

To increase the accuracy and effectiveness of focusing, particularly recently reported studies are performed with realistic magnetic resonance imaging (MRI)-based digital phantoms. Although it is important to perform optimization with such phantoms, the evaluation of electric fields in an in-homogeneous environment is challenging. Therefore, mostly FEM-based commercial software or in-house algorithms are used for the evaluation of electric fields. FEM-based methods, especially for dispersive and lossy environments, are suffering from both time and computational inefficiencies. The goal of this work is to overcome these challenges by modeling the breast medium with cylinders. Through this approach, analytical solution can be used to calculate the field distribution in the breast medium. The cylindrical of the medium allows the calculation of antenna phases with a very straightforward approach, which simply relies on maximizing the modulus of a complex quantity. Although the medium is simplified in previously reported studies with different approaches [17, 18], limitations and effectiveness of simplifying the medium have not been reported. Unlike the previous work, we propose a thorough analysis by simplifying the breast medium with three-layered eccentric cylinders and next compute the electric field distribution in terms of cylindrical harmonics using analytical approaches. A simple and robust optimization technique is then implemented to maximize the total electric field at the tumor region which is represented as the vector summation of complex quantities in terms of antenna phases. This work offers several advancements: (1) Simplified modeling: We introduce a three-layered, eccentric cylindrical breast model. This facilitates analytical methods, addressing computational and time-intensive constraints of traditional FEM techniques. (2) Excitation enhancement: We employ an innovative excitation phase optimization. This ensures electric fields intensify specifically around tumor areas. (3) Personalized approach: We incorporate patient uniqueness through a dielectric property (DP) averaging technique. Optimizations are based on DP averages from detailed breast phantoms. (4) Comprehensive evaluation: Our method's potential and limitations are explored by contrasting the phase results of our model with those from intricate breast tissue representations.

Utilization of the proposed technique is attractive due to, (a) straightforward implementation, (b) minimal computational and time cost, and (c) a simple and robust phase optimization scheme in which the phases are directly computed by taking one of the antenna phases as a reference. Towards this end, this work adopts a cylindrical microwave applicator surrounding the cylindrically modeled breast medium with eight individual circularly positioned line sources. The focus is achieved first by selecting a reference phase value for one of the excitation sources. Next, to maximize the vector sum at the desired point, the phases of the remaining excitation sources are directly calculated so as to be in-phase with the chosen reference phase value. To expand the application of the technique for different breast models, the DPs of the main cylinder is obtained from the realistic models and the phases are optimized accordingly. Lastly, calculated phase values are tested with the corresponding realistic digital breast phantoms and successful results are obtained. An extensive numerical analysis is given to test the approach under different circumstances. Lastly, calculated phases are evaluated with realistic digital phantoms.

The remainder of this paper is organized as follows: Problem configuration and approach are defined in Section 2, the results along with analysis are given in Section 3, conclusions are drawn in Section 4.

2. Problem statement and the method

This section describes the hyperthermia problem and demonstrates the hyperthermia applicator configuration. Moreover, a detailed explanation of analytical electric field modeling, phase optimization approach, and the DP averaging of the realistic breast medium is given.

2.1. Statement of the problem

Consider the microwave breast hyperthermia problem configuration illustrated in Figure 1a. Here the human breast is illuminated by N antennas excited by different phases positioned in a circular fashion surrounding the breast. For simplicity, the amplitudes of the antenna currents are assumed to be equal. The goal is to adjust the electric field distribution inside the breast region so that its amplitude at a target point is maximum. The target point ideally corresponds to the center of the malignant tumor. This will also ensure the maximum temperature at this point since the electromagnetic energy that will be converted into heat is proportional to $|E|^2$ and σ. It is well known that the conductivity values (σ) of malignant tumors are larger than that of healthy tissues and it is an inherent property of the tissue [25]. Therefore, the main aim of the hyperthermia problem at hand becomes the optimization of the antenna phase values in order to maximize the electric field at the center of the malignant tumor. This problem can be cast as a nonlinear optimization problem [26, 27]. Although a limited number of simplified approaches have been reported [28], the majority of the presented studies [29–31] relies on slow optimization techniques in conjunction with computationally demanding full-wave analysis of the breast medium.

2.2. Evaluation of the focusing effectiveness with realistic fatty breast phantom

In the present study, it is shown that the optimization of the antenna phases can be effortlessly achieved by utilizing a simplified human breast model. This model consists of eccentric homogeneous cylinders which allow the calculation of the field distribution analytically. In the following sections, the simplified cylindrical breast model, patient-specific DP calculation to homogenize the medium, and the solution of the phase optimization problem are given in detail.

2.3. Hyperthermia problem with equivalent simplified cylindrical structure

The two-dimensional (2D) cross-section view of the heterogeneous model along with circular hyperthermia applicator configuration for breast hyperthermia problem is shown in Figure 1a. The breast tissue in the hyperthermia problem is transformed into a homogeneous three-layered cylindrical model and it is shown in Figure 1b. The cross-sectional view given in Figure 1b represents skin, homogenized breast medium, and tumor. The outer cylinder DPs and radius are denoted with ε_s, σ_s, and ρ_s, respectively, which depict the skin. Inner concentric cylinder DPs and radius are denoted with ε_b, σ_b, and ρ_b, respectively, which represent the homogenized breast medium. Finally, the off-center cylinder with a much smaller radius (ρ_t) was inserted into the breast to represent the malignant tumor DPs denoted with ε_t, σ_t. Since the biological tissues are nonmagnetic, all tissues in the cylindrical model have the permeability of free space (μ_0). Note that all DPs representing the skin, breast, and malignant tumor tissue was obtained using the single-pole Debye model with parameters given in [32].

2.4. Dielectric property (DP) approximation for homogenized breast medium

In this work, two types of realistic breast models obtained from MRI are considered. $Class-II$ type of breast with 012204 ID is classified as a fatty breast model and $Class-III$ type of breast with 062204 ID is classified as a very dense breast model. Both models are obtained from [33].

Using the approach proposed in [15], the DPs of the homogenized breast represented with the second concentric cylinder (ρ_b) in Figure 1b are calculated. This approach essentially homogenized the heterogeneous

healthy breast tissue in the realistic model. To execute this method, we initially obtain a cross-section from each breast model at $z = 0$. Next, the thickness of the skin in each MRI model is calculated. Since the skin is represented with an outer cylinder, the skin DPs are omitted during the calculation of DPs for the homogenized cylinder. In the simplified model, the thickness of the outer cylinder $(\rho_s - \rho_b)$ approximately has the same thickness as the skin in the realistic breast slice.
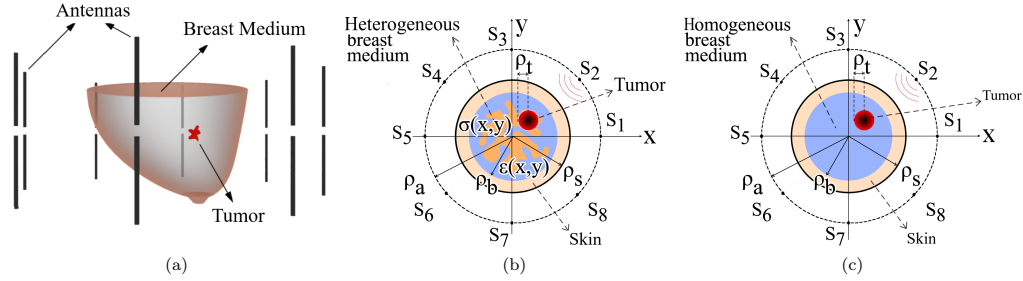

Figure 1. Microwave breast cancer hyperthermia problem configuration. Subfigures are: (a) 3D problem representation, (b) problem cross-section and configured system with realistic breast tissue, (c) the equivalent simplified eccentric homogeneous cylindrical configuration with layers representing skin, homogenized breast medium, and tumor.

In order to calculate the DPs of the homogenized breast medium, the spatial mean of DPs, namely dielectric constant $\varepsilon(x, y)$ and conductivity $\sigma(x, y)$, in the realistic breast medium are calculated with the following equations:

$$\varepsilon_b = \frac{1}{S} \iint \varepsilon(x, y) \, dx \, dy \tag{1}$$

$$\sigma_b = \frac{1}{S} \iint \sigma(x, y) \, dx \, dy \tag{2}$$

where S is the total area of the breast medium cross-section excluding skin. Also, tumor inclusion is not considered during the spacial mean calculation of heterogeneous medium DPs. Using the above equations, the spacial mean DPs of the heterogeneous breast medium composed of fat and fibroglandular tissues are calculated and assigned to the second concentric cylinder with ρ_b radius shown in Figure 1b. The calculated dielectric properties for fatty breasts with 012204 ID are $\varepsilon_b = 7.82$ and $\sigma_b = 0.37$ and for dense breasts with 062204 ID are $\varepsilon_b = 15.76$ and $\sigma_b = 0.92$ at 4 GHz.

2.5. Modelling of the sources and field distribution

In order to focus the EM field to a desired point inside the breast, 8 line source is placed on a circle with $45°$ angular distance and the same distance from the center of the circle. It is assumed that each line source has the same amplitude. The phase of one of the 8 line sources is chosen as the reference. For simplicity, the first antenna is chosen with a reference phase zero (0). Note that this choice does not affect the solution. The total incident field at any point outside the breast medium can be written as follows:

1

$$E^i(x) = \sum_{m=1}^{8} -\frac{\eta_0 k_0 I_0}{4} e^{j\varphi_m} H_0^{(2)}(k_0|x - y^{(m)}|) \tag{3}$$

where $H_0^{(2)}$ is the Hankel function of the 2nd kind with zero order, $x = (x_1, x_2)$ and $y^{(m)} = (y_1^{(m)}, y_2^{(m)})$ are the observation point and the location of the mth source in $2D$ space, respectively. In equation (3), $k_0 = \omega\sqrt{\varepsilon_0\mu_0}$ is the wave number of the free space, $\eta_0 = \sqrt{\frac{\mu_0}{\varepsilon_0}}$ is the intrinsic impedance of the free space, I_0 is the current strength of the line sources and φ_m is the phase of the mth line source, where $m = 1, 2, ..., 8$. The addition theorem for cylindrical harmonics can be used to express the incident field in the region $\rho_s < \rho < \rho_a$ as;

$$E^i(\rho, \phi) = -\frac{\eta_0 k_0 I_0}{4} \sum_{m=1}^{8} e^{j\varphi_m} \sum_{n=-\infty}^{\infty} H_n^{(2)}(k_0\rho_a) J_n(k_0\rho) e^{jn(\phi-\phi_m)}, \quad \rho_s < \rho < \rho_a \tag{4}$$

where (ρ, ϕ) denotes the cylindrical coordinates, (ρ_a, ϕ_m) is the location of mth source, $m = 1, 2, ..., 8$. $H_n^{(2)}$ and J_n are the Hankel function of the second kind with n^{th} order and the Bessel function of the nth order, respectively. The total field inside and outside the breast region can now be written through the use of the shifted cylindrical coordinates (ρ', ϕ'), where the center for this new system is taken as the center of the off-centered circle inside the breast representing the tumor in the cross-section given in Figure 1b. Thus, one can represent the total field in the whole space as:

$$E = \left(-\frac{\eta_0 k_0 I_0}{4}\right) \begin{cases} \sum_{m=1}^{8} e^{j\varphi_m} \sum_{n=-\infty}^{\infty} \left[H_n^{(2)}(k_0\rho_a)J_n(k_0\rho) + a_n^m H_n^{(2)}(k_0\rho)\right] e^{jn(\phi-\phi_m)}, & \rho_s < \rho < \rho_a \\ \sum_{m=1}^{8} e^{j\varphi_m} \sum_{n=-\infty}^{\infty} \left[b_n^m J_n(k_1\rho) + c_n^m H_n^{(2)}(k_1\rho)\right] e^{jn\phi}, & \rho_b < \rho < \rho_s \\ \sum_{m=1}^{8} e^{j\varphi_m} \sum_{n=-\infty}^{\infty} \left[d_n^m J_n(k_2\rho') + e_n^m H_n^{(2)}(k_2\rho')\right] e^{jn\phi'}, & \rho < \rho_b, \rho' > \rho_t \\ \sum_{m=1}^{8} e^{j\varphi_m} \sum_{n=-\infty}^{\infty} \left[f_n^m J_n(k_3\rho')\right] e^{jn\phi'}, & \rho' < \rho_t \end{cases} \tag{5}$$

where a_n^m, b_n^m, c_n^m, d_n^m, e_n^m, and f_n^m are unknown coefficients that need to be determined.

Using the appropriate boundary conditions together with coordinate transformations, one can determine the unknown coefficients, by following the method given in [34]. The method is based on the application of the addition theorem in conjunction with an appropriate coordinate transformation. Then one can easily apply the boundary conditions on the surfaces of the inner and outer cylinders to reduce the problem to the solution of an infinite dimensional matrix equation which is solved by truncation of the system [34]. The field inside the tumor circle can now be determined by using the coefficients f_n^m appearing in equation (5). Eventually, those coefficients will be used in the phase optimization algorithm, which will be given in the next section.

2.6. Phase optimization approach based on maximization of the vector sum at the target point

Consider the electric field at the center of the small circle shown in the cross-section given with Figure 1b, which coincides with the center of the malignant tumor. It is denoted as E_{tumor}. We define the central point

of the tumor circle as a focus point denoted by (x_f, y_f). Then, ρ_f and ϕ_f forms as $\rho_f = \sqrt{x_f^2 + y_f^2}$ and $\phi_f = tan^{-1}(y_f/x_f)$, with respect to the shifted origin. Taking (5) into account, E_{tumor} can be written as follows:

$$E_{tumor} = -\frac{\eta_0 k_0 I_0}{4} \sum_{m=1}^{8} e^{j\varphi_m} \sum_{n=-\infty}^{\infty} f_n^m J_n(k_3 \rho_f) e^{jn\phi_f} \tag{6}$$

Let us define A_m as,

$$A_m = -\frac{\eta_0 k_0 I_0}{4} \sum_{n=-\infty}^{\infty} f_n^m J_n(k_3 \rho_f) e^{jn\phi_f} \tag{7}$$

It is obvious that (6) is a complex quantity and since it is desired to maximize the magnitude of this expression, we can simply define an extremum problem in terms of the unknown phase values of the line sources. To this aim, we define the following function which is the square of the magnitude of E_{tumor} as a function of unknown phase values.

$$f(\varphi_1, \varphi_2, \varphi_3, \varphi_4, \varphi_5, \varphi_6, \varphi_7, \varphi_8) = E_{tumor} E_{tumor}^*$$
$$= \left| \sum_{m=1}^{8} e^{j\varphi_m} A_m \right|^2 \tag{8}$$

The phase optimization problem can now be defined in a much more compact form as:

Determine $\tilde{\varphi}$ so that $f(\tilde{\varphi}) \to$ max.

where $\tilde{\varphi} = (\varphi_1, \varphi_2, \varphi_3, \varphi_4, \varphi_5, \varphi_6, \varphi_7, \varphi_8)$ is considered as vector in 8 dimensional Euclidean space.

Now, let us write f in the following explicit form:

$$f(\tilde{\varphi}) = \left| A_1 e^{j\varphi_1} + A_2 e^{j\varphi_2} + ... + A_8 e^{j\varphi_8} \right|^2 \tag{9}$$

The phase of the first antenna (φ_1) is set to $0°$ as a reference, and in order to maximize the quantity given in (9), the phases of the field at the center of the tumor due to remaining antennas should be equal to the phase of the expression (A_1) formed by the first antenna.

$$Arg(A_1) = Arg(A_2 e^{j\varphi_2}) = ... = Arg(A_8 e^{j\varphi_8}) \tag{10}$$

Then, the phases of the remaining antennas can now be obtained as follows:

$$\varphi_k = Arg(A_1) - Arg(A_k) \tag{11}$$

where $k = 2, 3, ..., 8$

Because of the indefiniteness of argument of complex quantities, phase of the each antenna is set to stay between $[-\pi, \pi]$ interval.

3. Results and discussion

The methodology described in Section 2.6 is implemented for two cylindrical configurations shown in Figure 1b. The dimensions of these configurations are $\rho_s = 55.7\ mm$, $\rho_b = 52.2\ mm$ for $Class - II$ type of breast with the 012204 ID and $\rho_s = 40.1\ mm$, $\rho_b = 38.6\ mm$ for $Class - III$ type of breast with the 062204 ID. The radius of the tumor is $\rho_t = 5\ mm$ for both configurations. The difference between the two configurations is that the first one mimicked a fatty breast and the second mimicked a dense breast. To implement the method, first, phantom models obtained from [33] are imported to both MATLAB and computer simulation technology (CST) software. Next, spacial averaged DPs of the breast medium are calculated to homogenize each model. Subsequently, the DPs of skin, homogenized breast medium, and tumor dielectric properties are assigned. Both configurations are illuminated with 8 line sources which are placed $80\ mm$ away from the center of the breast medium. They are separated with $45°$ angle in a circular manner as shown in Figure 1b. After setting the breast configuration, the phases are obtained using the optimization approach given in Section 2.6.

Next, using the phases obtained from the homogenized phantom, the corresponding realistic inhomogeneous breast phantom is illuminated with the same antenna to perform the electric field, energy, and heat distribution analysis. To this aim, first, the amplitude of the electric field inside the breast phantoms for both realistic $Class - II$ with 012204 ID and $Class - III$ with 062204 ID types, namely fatty and dense, are calculated using an in-house method of moments (MoM) technique in MATLAB. Note that $I_0 = 1\ A$, frequency is selected as 4 GHz, the background is assigned as air with $\varepsilon_r = 1$, and the background cell dimensions in 2D MoM analysis are set to $0.5\ x\ 0.5\ mm^2$.

The antenna phases obtained through the optimization with a simplified model were also used in CST for both realistic breasts to produce temperature distribution. In CST, a sphere with a radius of 5 mm is placed to mimic the malignant tumor tissue. The dipole antennas are placed as in Figure 1a and driven with a Gaussian signal with the normalized amplitude. During the thermal analysis in CST, thermal parameters given in [15] are used. A cooling medium outside the digital phantoms is also applied during thermal analysis. The convection boundary condition is applied on the skin with the convection coefficient of $200\ W/m^2\ °C$ and the temperature of $25°C$ in order to prevent the skin from overheating. For a better comparison of the given results, two metrics are calculated. One is the Euclidean 2-D distance between the target point and the maximum point of power density or temperature. The desired focus point coordinates are shown with (x_f, y_f), and (x_m, y_m) denotes the coordinates of the obtained maximum power density or the maximum temperature. The second calculated metric is the ratio of the total power density of the tumor cells and healthy cells denoted with $Q_{tumor}/Q_{healthy}$ and it is defined in (12)

$$Q_{tumor}/Q_{healthy} = \frac{\frac{\iint\limits_{S_{tumor}} \sigma(x,y)|E(x,y)|^2\,dxdy}{S_{tumor}}}{\frac{\iint\limits_{S_{healthy}} \sigma(x,y)|E(x,y)|^2\,dxdy}{S_{healthy}}} \tag{12}$$

where S_{tumor} and $S_{healthy}$ denote the cross-sectional area of the tumor and the cross-sectional area of healthy tissues, respectively. Finally, it should be emphasized that all results are given on the $z = 0$ plane. The remainder of this section reports the obtained results in detail.

3.1. Evaluation of the focusing effectiveness with realistic fatty breast phantom

The tumor inclusion with 5 mm radius is placed at two locations in the simplified homogeneous cylindrical model mimicking the $Class-II$ type with 012204 ID fatty breast phantom. The two locations are $(x, y) = (13.3, 20.2)$ mm named case-1 and $(x, y) = (-24.8, -12.1)$ mm named case-2. The phase values for each location are obtained using the analytical modeling of the fields inside the homogenized cylindrical model along with the optimization approach given in Section 2.6. Next, phases obtained from the simplified model are used in MoM and CST with the realistic fatty model ($Class-II$ ID 012204 breast) to obtain field, power density, and temperature distributions. Obtained results case-1, namely for $(x, y) = (13.3, 20.2)$ mm are shown in Figure 2. Comparing the amplitude of the electric field distribution with and without optimization in Figures 2a and 2b, it can be seen that the field strength increases significantly at the tumor when optimization is applied. Similarly, a comparison of Figures 2c and 2d shows that microwave power density increases in direct proportion to the amplitude of the electric field.

Table 1. A comparison of power density ratio results between the tumor and healthy tissue ($Q_{tumor}/Q_{healthy}$) obtained from in-house simulations for fatty $Class-II$ ID 012204 breast along with the distance between the target focus point (x_f, y_f) and obtained maximum power density (x_m, y_m).

Breast type	(x_f, y_f) (mm)	(x_m, y_m) (mm)	Distance (mm)	$Q_{tumor}/Q_{healthy}$
Fatty - case-1	(13.3,20.2)	(13.3,20.5)	0.3	0.61
Fatty - case-2	(-19.1,-12.1)	(-25.7,-13.0)	26	0.27

In Table 1, the target focus point (x_f, y_f), the point (x_m, y_m) where the maximum power density is obtained and the distance between the two points are given. Similarly, the power density ratio results between the tumor and healthy tissue ($Q_{tumor}/Q_{healthy}$) are given for two locations. It is shown in Table 1 that for case-1 the focusing is achieved with 0.3 mm shift from the target location with a 0.61 power density ratio.

In the next step, case-1 is evaluated in CST with $Class-II$ type with 012204 ID fatty realistic breast phantom. In Figures 2e and 2f, the temperature distributions obtained with the optimized phase values are shown. We note that the appropriate power factor is set to 15 and power radiated from each antenna is increased to 6W in order to reach the desired temperature on the tumor for both fatty and dense cases during CST simulations. From Figure 2e, it can be seen that the maximum temperature occurs inside the tumor inclusion. However, some of the healthy tissues are also heated up to $40°C$. We try to overcome this unwanted outcome by turning off the furthest three antennas away from the tumor using the approach proposed in [9]. Through this process, the number of active antennas is reduced to 5 from 8. The results after this process are shown in Figure 2f. As shown in Table 2, the maximum point of temperature occurs only at a 1.3 mm distance from the focus for both 8 and 5 antennas.

Next, we move on to a more challenging scenario, case-2, for fatty breast. Here, the malignant tumor is located on the glandular tissue which has very similar DPs to the malignant tumor inclusion. The MoM results of case-2 are shown in Figure 3. As seen from Figures 3a and 3b, with the optimized phase values, the amplitude of the electric field increased and it is concentrated inside the tumor. It is clear from Figures 3c and 3d, power density is concentrated inside the tumor by focusing the amplitude of the electric field on the center of the tumor. From Figure 3d, it can be seen that 26 mm shift from the target location with 0.27 power density ratio for case-2 are obtained.
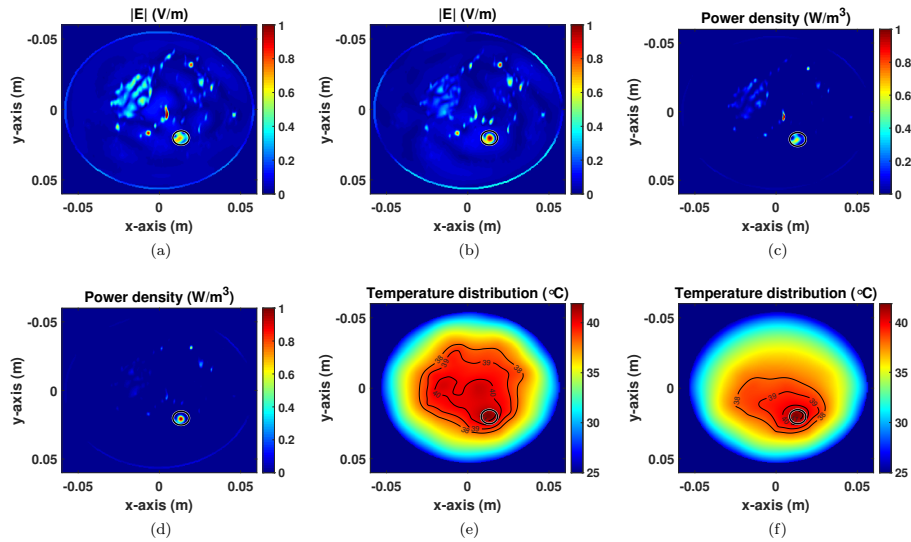
Figure 2. The distribution of normalized electric field amplitude, microwave power, and temperature for a $Class - II$ breast model, calculated at $(x, y) = (13.3, 20.2)$ mm via MoM and CST software. It presents both optimized and unoptimized antenna phase scenarios. Subfigures are: (a) electric field distribution without optimization, (b) electric field distribution with optimization, (c) power density without optimization, (d) power density with optimization, (e) temperature distribution, and (f) temperature distribution with the furthest three antennas deactivated.

Table 2. A comparison of temperature peak obtained from CST Simulations for fatty $Class - II$ ID 012204 breast along with the distance between the target point (x_f, y_f) and obtained maximum temperature point (x_m, y_m).

Breast type	Antenna status	(x_f, y_f) (mm)	(x_m, y_m) (mm)	Distance (mm)
Fatty - case-1	On	(13.3,20.2)	(12.3,19.5)	1.3
Fatty - case-1	S_6, S_7, S_8 Off	(13.3,20.2)	(12.3,19.5)	1.3
Fatty - case-2	On	(-19.1,-12.1)	(-12.8,-8.0)	7.6
Fatty - case-2	S_1, S_7, S_8 Off	(-19.1,-12.1)	(-21.3,-10.0)	3

The results obtained from the CST are given in Figure 3, and the maximum temperature is shifted 7.6 mm from the tumor center according to Figure 3e. Next, the furthest three antennas from the center of the tumor are shut down. The temperature distribution obtained with the remaining 5 antennas is illustrated in Figure 3f. It can be seen that higher temperature values are obtained inside the tumor and the temperature shift is decreased to 3 mm. The results are also given in Table 2.

3.2. Evaluation of the focusing effectiveness with realistic dense breast phantom

In order to see the focusing performance for the realistic dense breast, previously described steps are applied to the dense breast model which is classified as $Class - III$ type with 062204 ID. The tumor inclusion has a radius of 0.5 mm and is placed at $(x, y) = (-13.4, -8.5)$ mm and $(x, y) = (15, 3.6)$ mm named case-3 and case-4, respectively.
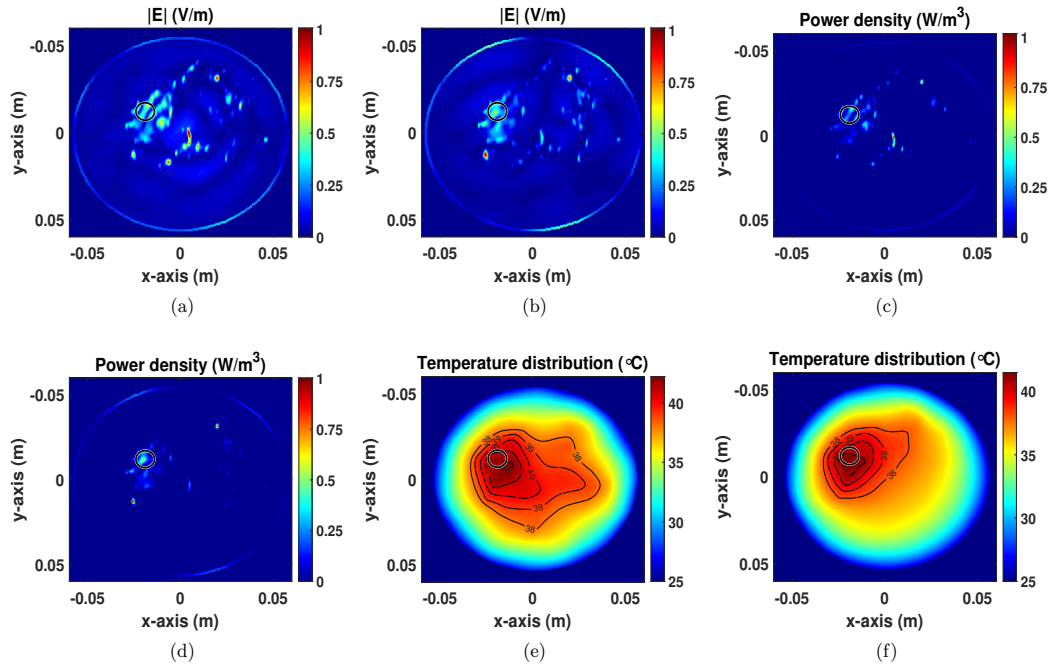
Figure 3. The distribution of normalized electric field amplitude, microwave power, and temperature for a $Class - II$ breast model, calculated at $(x, y) = (-24.8, -12.1)$ mm via MoM and CST software. It presents both optimized and unoptimized antenna phase scenarios. Subfigures are: (a) electric field distribution without optimization, (b) electric field distribution with optimization, (c) power density without optimization, (d) power density with optimization, (e) temperature distribution, and (f) temperature distribution with the furthest three antennas deactivated.

Results for the case-3 are shown in Figures 4a and 4b. Using the optimized phase values, the amplitude of the electric field increased significantly on the tumor as shown in Figures 4a and 4b. Since the power density is directly proportional to the electric field, it can be seen from the Figures 4c and 4d that the power density is maximum at the center of the tumor. Distance between the desired maximum power density point and obtained maximum power density occurring in MoM simulations is 3.7 mm as given in Table 3. Obtained $Q_{tumor}/Q_{healthy}$ ratio is 0.55 which means around 35% power density concentrated inside the tumor inclusion compared to the whole breast.

Table 3. A comparison of power density ratio results between the tumor and healthy tissue ($Q_{tumor}/Q_{healthy}$) obtained from in-house simulations for dense $Class - III$ ID 062204 breast along with the distance between the target focus point (x_f, y_f) and obtained maximum power density (x_m, y_m).

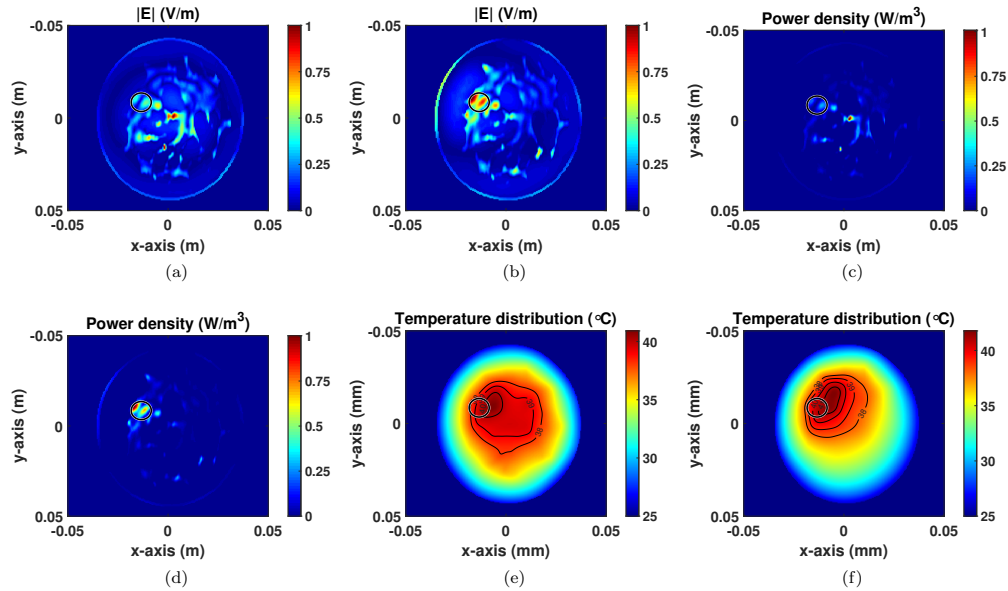| Breast type	(x_f, y_f) (mm)	(x_m, y_m) (mm)	Distance (mm)	$Q_{tumor}/Q_{healthy}$
Dense - case-3	(-13.4,-8.5)	(-16.5,-10.5)	3.7	0.55
Dense - case-4	(15.0,3.6)	(23.0,19.0)	17.4	0.082

Figure 4. The distribution of normalized electric field amplitude, microwave power, and temperature for a $Class - III$ breast model, calculated at $(x, y) = (-13.4, -8.5)$ mm via MoM and CST software. It presents both optimized and unoptimized antenna phase scenarios. Subfigures are: (a) electric field distribution without optimization, (b) electric field distribution with optimization, (c) power density without optimization, (d) power density with optimization, (e) temperature distribution, and (f) temperature distribution with the furthest three antennas deactivated.

Temperature distribution for optimized antenna phase values is shown in Figure 4e, and it can be seen that temperature distribution is spread rather than focusing inside the tumor inclusion. In order to prevent possible hot spots and shift the focus to inside the tumor inclusion, the antennas located at the furthest distance from the tumor canter are again turned off. The obtained temperature distribution with the remaining 5 antennas is shown in Figure 4f where the maximum temperature is still outside the tumor. However, the distance between the focus point and the maximum point decreases from 6.9 mm to 5.25 mm by 23.9 % as shown in Table 4.

For case-4 dielectric properties of tumor and glandular tissue are similar to one another which makes it harder to focus the electric field. MoM results for this simulation are presented in Figures 5a–5d. As seen from the figures, with the optimization process, the maximum values for electric field and power density do not change significantly, but the focus is shifted to the tumor side. For CST results as depicted in Figure 5e, the maximum temperature is obtained outside the tumor inclusion similar to the MoM results. By turning off the furthest three antennas from the tumor, although the maximum power is still outside the tumor, more power is concentrated in tumor inclusion. As a consequence of that, the maximum temperature is shifted inside the tumor location and reaches the $41°C$ as seen from the Figure 5f.

From Table 3, the shift from the desired focus point is 17.4 mm and the ratio of $Q_{tumor}/Q_{healthy}$ is 0.082. As predicted from the MoM results, in CST analysis, when all 8 antennas are working, the maximum point of temperature distribution occurs at a distance of 8.3 mm from the desired focus point, as seen from Table 4. Moreover, turning off the farthest three antennas decreases the distance around 81.93 % to 1.5 mm. With this approach, the maximum point of temperature occurs inside the tumor inclusion.

Table 4. A comparison of power density ratio results between the tumor and healthy tissue ($Q_{tumor}/Q_{healthy}$) obtained from CST Simulations for fatty $Class-II$ ID 012204 breast dense $Class-III$ ID 062204 breast along with the distance between the target focus point (x_f, y_f) and obtained maximum power density (x_m, y_m).

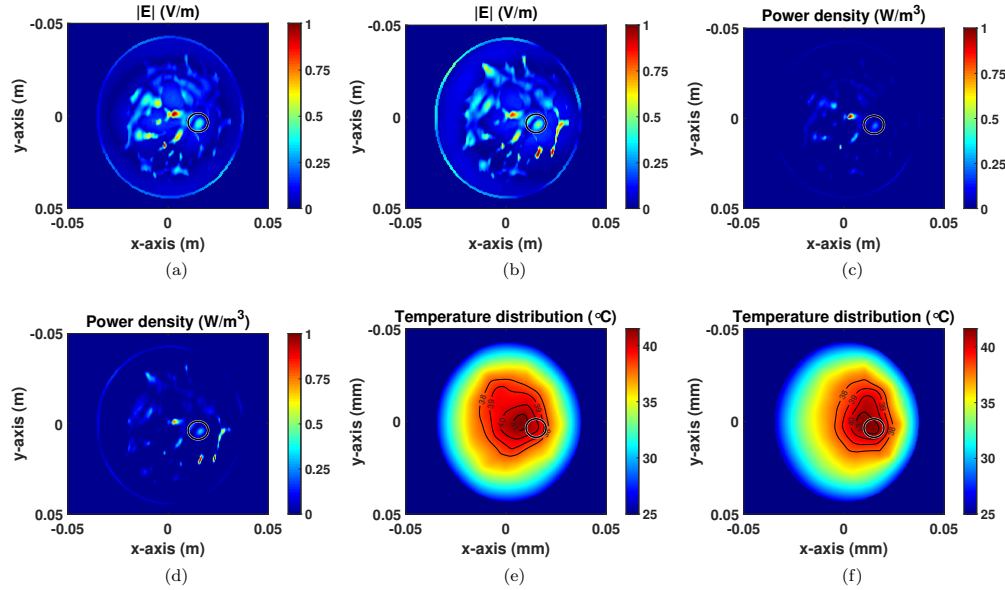| Breast type	Antenna status	(x_f, y_f) (mm)	(x_m, y_m) (mm)	Distance (mm)
Dense	On	(-13.4,-8.5)	(-6.5,-9.0)	6.9
Dense	S_1, S_7, S_8 Off	(-13.4,-8.5)	(-10.0,-12.5)	5.25
Dense	On	(15.0,3.6)	(7.5,0.0)	8.3
Dense	S_5, S_6, S_7 Off	(15.0,3.6)	(13.5,3.0)	1.5

Figure 5. The distribution of normalized electric field amplitude, microwave power, and temperature for a $Class-III$ breast model, calculated at $(x, y) = (15, 3.6)$ mm via MoM and CST software. It presents both optimized and unoptimized antenna phase scenarios. Subfigures are: (a) electric field distribution without optimization, (b) electric field distribution with optimization, (c) power density without optimization, (d) power density with optimization, (e) temperature distribution, and (f) temperature distribution with the furthest three antennas deactivated.

Regarding the safety limits, there are no specific safety limits for breast cancer hyperthermia. Having said that, in the context of hyperthermia research, two common limitations are often discussed, and they can be considered safety-related limitations: (1) According to [35], the most important issue is to eliminate the heating of the skin, (2) limiting the energy deposition at the remaining healthy tissue within the breast medium to prevent hot spots.

In our frequency of operation, power deposition to the skin tissue surrounding the breast is inevitable due to the high inherent conductivity of the skin. However, the temperature can be controlled by using a cooling medium. We implemented a cooling medium with 25 ℃ to prevent overheating of the skin. Next, to mitigate the hot spots in healthy tissue, we shut down the furthest three antennas away from the tumor. We can attempt

to evaluate the safety of our system by comparing the total power deposited by our system to the previously reported ones. In [36], for a system operating between 300 and 6000 MHz, the maximum power density for 4 GHz is calculated as 7.58 W/m^2 for continuous exposure systems and 40.82 W/m^2 for timed exposure systems. In our study, for Case 1, the total power density of the system is calculated as 9.7 W/m^2, but when the furthest three antennas shut down, it decreased to 6 W/m^2, which is below the power limits reported in [36]. For Case 2, the total power density of the system is calculated as 8.93 W/m^2, but when the furthest three antennas are shut down, it decreased to 5.4 W/m^2, which is again below the calculated power reported in [36]. For dense breast, Case 3, the total power density of the system is calculated as 7.99 W/m^2, but when the furthest three antennas shut down, it decreased to 4.53 W/m^2, which is below the power levels reported in [36]. Finally, for Case 4, the total power density of the system is calculated as 4.42 W/m^2, but when furthest three antennas shut down, it decreased to 3.35 W/m^2, which is below the previously reported power levels in [36]. In [36], SAR limit is reported as 20 W/kg for timed exposure system. When all antennas are operating, for Case 1, Case 2, Case 3, and Case 4, the SAR is calculated as 20 W/kg, 18.41 W/kg, 16.47 W/kg, and 9.11 W/kg, respectively. When the furthest three antennas are shut down, for Case 1, Case 2, Case 3, and Case 4, the SAR is calculated as 12.37 W/kg, 11.13 W/kg, 9.34 W/kg, and 6.9 W/kg, respectively. As shown in the calculations above, for all four cases, the SAR deposition in our system does not exceeded the SAR limit.

4. Conclusions

This work presents a fast and effective phase optimization approach for breast cancer hyperthermia treatment. Through modeling the breast tissue as a cylindrical medium, the field distribution was obtained using an analytical solution approach. Once the field distribution is expressed in the target medium with cylindrical harmonics, the field strength is maximized at the desired point via a simple vector optimization of the source phases. It was concluded that the obtained phases perform well when contrast difference occurs for dielectric and thermal properties between the malignant tumor and surrounding breast tissue. When the tumor inclusion is located in the fibroglandular tissue, the shift of temperature focus is significantly improved by turning off the farthest three antennas. The proposed technique shows promising results for rapid optimization of the antenna phases.

References

[1] Amichetti M, Valdagni R, Graiff C, Valentini A. Local-regional recurrences of breast cancer: treatment with radiation therapy and local microwave hyperthermia. American Journal of Clinical Oncology 1991; 14 (1): 60–65. https://doi.org/10.1097/00000421-199102000-00014

[2] Li X, Zhang X, Khan IU, Guo NN, Wang B et al. The anti-tumor effects of the combination of microwave hyperthermia and lobaplatin against breast cancer cells in vitro and in vivo. Bioscience Reports 2021; 42 (2): 1-24. https://doi.org/10.1042/BSR20190878

[3] Gee W, Lee SW, Bong NK, Cain CA, Mittra R et al. Focused Array Hyperthermia Applicator: Theory and Experiment. IEEE Transactions on Biomedical Engineering 1984; 31 (1): 38-46. https://doi.org/10.1109/TBME.1984.325368

[4] Fenn AJ, Wolf GL, Fogle RM. An adaptive microwave phased array for targeted heating of deep tumours in intact breast: animal study results. International Journal of Hyperthermia 1999; 15 (1): 45–61. https://doi.org/10.1080/026567399285846

[5] Issels RD. Hyperthermia adds to chemotherapy. European journal of cancer 2008; 44 (17): 2546–2554. https://doi.org/10.1016/j.ejca.2008.07.038

[6] Altintas G, Akduman I, Janjic A, Yilmaz T. A novel approach on microwave hyperthermia. Diagnostics 2021; 11 (3): 493-503. https://doi.org/10.3390/diagnostics11030493

[7] Yildiz G, Yasar H, Uslu IE, Demirel Y, Akinci MN et al. Antenna excitation optimization with deep learning for microwave breast cancer hyperthermia. Sensors 2022; 22 (17): 6343-6358. https://doi.org/10.3390/s22176343

[8] Yildiz G, Yilmaz T, Akduman I. Rotationally adjustable hyperthermia applicators: A computational comparative study of circular and linear array applicators. Diagnostics 2022; 12 (11): 2677-2690. https://doi.org/10.3390/diagnostics12112677

[9] Nguyen PT, Abbosh A, Crozier S. Microwave hyperthermia for breast cancer treatment using electromagnetic and thermal focusing tested on realistic breast models and antenna arrays. IEEE Transactions on Antennas and Propagation 2015; 63 (10): 4426–4434. https://doi.org/10.1109/TAP.2015.2463681

[10] Nguyen PT, Abbosh AM, Crozier S. 3-d focused microwave hyperthermia for breast cancer treatment with experimental validation. IEEE Transactions on Antennas and Propagation 2017; 65 (7): 3489–3500. https://doi.org/10.1109/TAP.2017.2700164

[11] Xu L, Wang X. Focused microwave breast hyperthermia monitored by thermoacoustic imaging: A computational feasibility study applying realistic breast phantoms. IEEE Journal of Electromagnetics, RF and Microwaves in Medicine and Biology 2019; 4 (2): 81–88. https://doi.org/10.1109/JERM.2019.2931623

[12] Li J, Wang B, Zhang D, Li C, Zhu Y et al. A preclinical system prototype for focused microwave breast hyperthermia guided by compressive thermoacoustic tomography. IEEE Transactions on Biomedical Engineering 2021; 68 (7): 2289 - 2300. https://doi.org/10.1109/TBME.2021.3059869

[13] Asili M, Chen P, Hood AZ, Pursuer A, Hulsey R et al. Flexible microwave antenna applicator for chemo-thermotherapy of the breast. IEEE Antennas and Wireless Propagation Letters 2015; 14: 1778–1781. https://doi.org/10.1109/LAWP.2015.2423655

[14] Converse M, Bond EJ, Veen BD, Hagness C. A computational study of ultra-wideband versus narrowband microwave hyperthermia for breast cancer treatment. IEEE Transactions on Microwave Theory and Techniques, May 2006; 54 (5): 2169–2180. https://doi.org/10.1109/TMTT.2006.872790

[15] Zastrow E, Hagness SC, Van Veen BD. 3d computational study of non-invasive patient-specific microwave hyperthermia treatment of breast cancer. Physics in Medicine and Biology 2010; 55 (13): 3611-3431. https://doi.org/10.1088/0031-9155/55/13/003

[16] Iero DAM, Iserna T, Morabito AF, Catapano I. Optimal constrained field focusing for hyperthermia cancer therapy: A feasibility assessment on realistic phantoms. Progress In Electromagnetics Research 2010; 102: 125–141. https://doi.org/10.2528/PIER10011207

[17] Lim S, Yoon YJ. Lim S and Yoon YJ. Phase compensation technique for effective heat focusing in microwave hyperthermia systems. Applied Sciences 2021; 11 (13): 5972-5987. https://doi.org/10.3390/app11135972

[18] He X, Geyi W, Wang S. A hexagonal focused array for microwave hyperthermia: Optimal design and experiment. IEEE Antennas and Wireless Propagation Letters 2015; 15: 56–59. https://doi.org/10.1109/LAWP.2015.2429596

[19] Bellizi GG, Crocco L, Battaglia GM, Isernia T. Multi-frequency constrained sar focusing for patient specific hyperthermia. IEEE Journal of Electromagnetics, RF and Microwaves in Medicine and Biology 2017; 1: 74–80. https://doi.org/10.1109/JERM.2017.2766569

[20] Elkayal HA, Ismail NE, Lotfy M. Microwaves for breast cancer treatments. Alexandria Engineering Journal 2015; 54: 1105–1133. https://doi.org/10.1016/j.aej.2015.06.012

[21] Curto S, Garcia-Miquel A, Suh M, Vidal N, Lopez-Villegas JM et al. Design and characterisation of a phased antenna array for intact breast hyperthermia. International Journal of Hyperthermia 2017; 34: 250–260. https://doi.org/10.1080/02656736.2017.1337935

[22] Dooley WC, Vargas HI, Fenn AJ, Tomaselli MB, Harness JK. Focused microwave thermotherapy for preoperative treatment of invasive breast cancer: A review of clinical studies. Annals of Surgical Oncology 2009; 17: 1076–1093. https://doi.org/10.1245/s10434-009-0872-z

[23] Burfeindt MJ, Zastrow E, Hagness SC, Van Veen BD, Medow JE. Microwave beamforming for non-invasive patient-specific hyperthermia treatment of pediatric brain cancer. Physics in Medicine and Biology 2011; 56: 2743–2754. https://doi.org/10.1088/0031-9155/56/9/007

[24] Giombini A, Giovannini V, Cesare AD, Pacetti P, Ichinoseki-Sekine et al. Hyperthermia induced by microwave diathermy in the management of muscle and tendon injuries. British Medical Bulletin 2007; 83: 379–396. https://doi.org/10.1093/bmb/ldm020

[25] Martellosio A, Pasian M, Bozzi M, Perregrini L, Mazzanti A et al. Dielectric properties characterization from 0.5 to 50 ghz of breast cancer tissues. IEEE Transactions on Microwave Theory and Techniques 2016; 65 (3): 998–1011. https://doi.org/10.1109/TMTT.2016.2631162

[26] Weiser M. Optimization and identification in regional hyperthermia. International Journal of Applied Electromagnetics and Mechanics 2009; 30 (3-4): 265–275. https://doi.org/10.3233/JAE-2009-1027

[27] Köhler T, Maass P, Wust P, Seebass M. A fast algorithm to find optimal controls of multiantenna applicators in regional hyperthermia. Physics in Medicine and Biology 2001; 46 (9): 2503. https://doi.org/10.1088/0031-9155/46/9/318

[28] Arkadiusz M, Piotr G, Marcin S. Optimization of SAR coefficient for dipole antennas array with regard to local hyperthermia. In 2018 Applications of Electromagnetics in Modern Techniques and Medicine (PTZE); Raclawice, Poland; 2018. pp 1–4. https://doi.org/10.1109/PTZE.2018.8503175

[29] Trefna´ HD, Vrba J, Persson M. Time-reversal focusing in microwave hyperthermia for deep-seated tumors. Physics in Medicine and Biology 2010; 55 (8): 2167-2185. https://doi.org/10.1088/0031-9155/55/8/004

[30] Kosmas P, Zastrow E, Hagness SC, Van Veen BD. A computational study of time reversal techniques for ultra-wideband microwave hyperthermia treatment of breast cancer. In 2007 IEEE/SP 14th Workshop on Statistical Signal Processing; Madison, WI, USA; 2007. pp 312–316. https://doi.org/10.1109/SSP.2007.4301270

[31] Nguyen PT. Focusing microwave hyperthermia in realistic environment for breast cancer treatment. PhD, The University of Queensland, Brisbane, Australia, 2016. https://doi.org/10.14264/uql.2016.522

[32] Lazebnik M, Okoniewski M, Booske JH, Hagness SC. Highly accurate debye models for normal and malignant breast tissue dielectric properties at microwave frequencies. IEEE microwave and wireless components letters 2007; 17 (12): 822–824. https://doi.org/10.1109/LMWC.2007.910465

[33] Burfeindt MJ, Colgan TJ, Mays RO, Shea JD, Behdad N et al. MRI-derived 3-D-printed breast phantom for microwave breast imaging validation. IEEE antennas and wireless propagation letters, December 2012; 11: 1610-1613. https://doi.org/10.1109/LAWP.2012.2236293

[34] Ghavami N, Tiberi G, Edwards DJ, Safaai-Jazi A. Huygens principle based imaging of multilayered objects with inclusions. Progress In Electromagnetics Research 2014, 58: 139–149. https://doi.org/10.2528/PIERB13121002

[35] D'Andrea JA, Ziriax JM, Adair ER. Radio frequency electromagnetic fields: mild hyperthermia and safety standards. Progress In Brain Research 2007; 162: 107–135. https://doi.org/10.1016/S0079-6123(06)62007-4

[36] Consumer and Clinical Radiation Protection Bureau, Environmental and Radiation Health Sciences Directorate, Healthy Environments and Consumer Safety Branch, and Health Canada. Limits of human exposure to radiofrequency electromagnetic energy in the frequency range from 3 kHz to 300 gHz. Safety Code 6, 2015.